Dnr
2020-018376
Projektnr
P2020-90287
Energimyndighetens titel på projektet – svenska
Provborrning för kunskapsinsamling inför framtida energiutvinning genom djupgeotermi
Universitet/högskola/företag
Göteborg Energi Aktiebolag
Namn på projektledare
Anna Pärsdotter

Final report

# Geological and geothermal characterisation of drillhole GE-2 in Gothenburg

Version
1.4
Date
2023-01-18
Prepared by
Axel Sjöqvist, PhD
Mikael Tillberg, PhD

## Preface

This project was operated by Göteborg Energi Aktiebolag with funding from Energimyndigheten. Drilling was completed by Emil Thomson assisted by Lucas Alexanderson and with project management by David Nilsson from GEO-gruppen i Göteborg AB. Simon Rejkjär and Jan-Erik Rosberg from Lunds tekniska högskola conducted downhole logging. Johan Hogmalm at Göteborg universitet and Thomas Eliasson at Sveriges geologiska undersökning contributed to an earlier phase of the deep geothermal study project. Alexandra Angelbratt, Staffan Carlsson, and Anna Pärsdotter at Göteborg Energi AB were successive project managers for the GE-2 project.

## Table of contents

## Summary

To conduct investigations into the geological feasibility for enhanced geothermal systems (EGS) in Gothenburg, a second deep drillhole, GE-2, was drilled during 2 February–14 June 2022 near Pilegården in southern Gothenburg. The drillhole started with a 70° angle from the surface toward the northeast (55°) and reached a depth of 986.65 m, corresponding to a vertical depth of approximately 863 m below the surface. Two downhole surveys collected data 98 days after drilling had finished, including the temperature profile of the drillhole and acoustic imaging of the drillhole wall to identify fractures.

The occurrence of different rock types was described from visual observations of the drill core. The drill cores comprise different varieties of crystalline gneiss, typical of the bedrock in western Gothenburg. At a depth of 911 m, there is a transition to a different rock suite, consisting of gneissic granite with high geothermal heat production (RA granite), which occurs at a much shallower depth than previously anticipated.

The nature and frequency of natural fractures intersected by the drillhole were studied in detail by combining observations from the drill cores and acoustic drillhole images to evaluate the natural permeability of the bedrock. The fractures can be distinguished as three or four predominant fracture sets with distinct orientations and mineral coatings. The main encountered fracture orientation is largely parallel to planar structures in the gneisses. These fractures are smooth and contain fracture coating minerals that are prone to slip. A set of rough vertical fractures occurs mainly in the middle section of the drillhole. There is no obvious indication that the intersections of the different fracture sets represent areas of increased natural permeability in the bedrock that could be targeted for EGS.

The geothermal gradient between 200 metres below surface and the bottom of hole is 16.94 °C/km with an intercept value of 7.64 °C at surface level. The uncorrected heat flow density is estimated to be 53.4 mW/m$^2$. Given a target temperature of 120 °C, this would require the geothermal wells to reach depths greater than 6.6 km, which would currently make them the deepest EGS wells in the world. The operation of a conventional EGS at depths greater than 6 km in crystalline bedrock (in Finland) has encountered both technical and economic challenges, both during construction and operation. Therefore, under the current circumstances, there does not seem to be a reasonable prospect for EGS in Gothenburg. If new projects succeed in overcoming the technical obstacles that exist today, the techno-economic feasibility could be re-evaluated by more testing in the existing drillholes GE-1 and GE-2.

## Sammanfattning

För att undersöka de geologiska förutsättningarna för djupgeotermi (enhanced geothermal systems, EGS) i Göteborg, borrades ett andra djupborrhål, GE-2, under perioden 2 februari–14 juni 2022 nära Pilegården i södra Göteborg. Hålet borrades med en lutning på 70° från markytan mot nordöst (55°) och nådde ett djup på 986,65 m, vilket motsvarar ett vertikaldjup på ungefär 863 m under markytan. Två mätningar i borrhålet samlade in data 98 dagar efter borrningen avslutades, inklusive en temperaturprofil av borrhålet och akustisk avbildning av borrhålsväggen för att identifiera sprickor.

Förekomsten av olika bergarter beskrevs genom visuella observationer av borrkärnan. Borrkärnorna innehåller olika varianter av kristallin gnejs, typiska för berggrunden i västra Göteborg. På ett djup av ungefär 911 m finns en övergång till en annan bergartssvit, som består av gnejsig granit med hög geotermisk värmeproduktion (RA granit), vilken förekommer på ett mycket grundare djup än vad som tidigare har antagits.

Egenskaper och frekvensen av naturliga sprickor som passerades av borrhålet studerades i detalj genom att kombinera observationer från borrkärnan och borrhålsavbildning för att utvärdera den naturliga permeabiliteten av berggrunden. Sprickorna kan särskiljas i tre eller fyra huvudsakliga sprickgenerationer med distinkta riktningar och mineralfyllnader. Den huvudsakliga sprickriktningen i borrhålet är parallell med planstrukturer i gnejserna. Dessa sprickor är släta och innehåller sprickfyllnadsmineral som har låg friktion. En annan sprickgeneration med råa vertikala sprickor förekommer huvudsakligen i mittsektionen av borrhålet. Det finns ingen självklar indikation att skärningsområdet mellan dessa två sprickgenerationer är ett område med förhöjd naturlig permeabilitet i berggrunden som skulle kunna användas som målområde till ett EGS.

Den geotermiska gradienten mellan 200 meter under markytan och borrhålets botten är 16,94 °C/km med en skärningspunkt på 7,64 °C vid markytan. Det okorrigerade värdet på värmeflödestätheten uppskattas till 53,4 mW/m². Givet en måltemperatur på 120 °C, skulle detta kräva geotermiska brunnar ned till mer än 6,6 km djup, vilket i nuläget skulle vara de djupaste EGS brunnarna i världen. Driften av ett konventionellt EGS på mer än 6 km djup i kristallin berggrund (i Finland) har haft både tekniska och ekonomiska utmaningar för både konstruktion och drift. Därför förefaller det inte under nuvarande förutsättningar finnas en rimlig möjlighet för EGS i Göteborg. Om nya projekt lyckas överkomma de tekniska hinder som finns i dag, kan den tekno-ekonomiska genomförbarheten omprövas genom mer testning i de befintliga borrhålen GE-1 och GE-2.

# 1. Introduction

## 1.1 Previous work

Investigations into the feasible extraction of geothermal energy from the crystalline bedrock in western Sweden go back to the 1984–1995 Hot Dry Rock (HDR) project at the Fjällbacka test site, located approximately 110 km north of Gothenburg. At Fjällbacka, numerous experiments were conducted to study geological, hydrogeological, and hydromechanical aspects of the development of a HDR geothermal reservoir with the goal to create a heat-exchanging interface from hydraulically stimulated pre-existing natural fractures in the bedrock. The project concluded that the development of a HDR geothermal reservoir was uneconomic due to impeded fluid flow between the wells and large fluid losses (Wallroth *et al.*, 1999).

In 2020, Göteborg Energi AB conducted a Feasibility Study to investigate the possibility of developing a deep geothermal reservoir to extract geothermal energy from the bedrock underneath Gothenburg for district heating in the city (Angelbratt, 2020). The study concluded that although extraction of geothermal energy from a deep reservoir seems simple, case studies from different locations in the world demonstrate that the economical extraction depends strongly on the local geological conditions. To investigate the local geological feasibility, the drilling of two deep drillholes was suggested to study the heat production, geothermal gradient, and characteristics of permeable fracture zones in the bedrock (Angelbratt, 2020). The first deep drillhole GE-1 was drilled down to approximately 1000 metres depth in 2021.

The main results of the investigation of GE-1 are the average measured geothermal gradient of 15 °C/km between 100 and 1000 metres, the observation that fractures mainly are localised in narrow zones with higher fracture frequency separated by longer zones of low fracturing, and that large-scale structures in the bedrock at depth have more shallow dips (~45°) than structures observed at the surface (~50–60°) (Hogmalm *et al.*, 2021).

This report describes the investigations conducted in and around the second deep drillhole, GE-2.

## 1.2 Project aims

The main aim of this project is to study the occurrence and character of deep fractures in the bedrock underneath a fracture valley in Gothenburg, and to evaluate them as zones of pre-existing natural permeability in the bedrock that may be utilised in the development of a deep geothermal reservoir. Furthermore, the geothermal properties and large-scale structure of the bedrock will be investigated to make predictions about the local thermal conditions and occurrence of geological structures at target depths typical for deep enhanced geothermal energy systems.

# 2. Geothermics and Enhanced Geothermal Systems

The Earth's interior is hot. Humans have since prehistoric times imagined the Earth's interior as a hot place from observations of volcanic eruptions, hot springs, and increasing temperatures in deep caves. In modern times, measurements of temperatures in deep drillholes, the development of better models of the Earth's physical and chemical structure, and measurements of geoneutrinos have increased our understanding of the heat flow in the Earth, but there are still large uncertainties in the field.

## 2.1 Sources and propagation of geothermal heat

The total heat flow that radiates out from the Earth's surface is approximately 43–49 TW. This heat has two main sources. A substantial but difficult-to-define proportion consists of **primordial heat** from the formation and early development of the Earth at 4.6 billion years ago, segregation of the Earth's metallic core from the silicate mantle, and heat production from extinct short-lived radioactive isotopes. The second source is the continuous and ongoing energy release by the long-lived **radioactive decay** of primarily uranium-238 ($^{238}$U), uranium-235 ($^{235}$U), thorium-232 ($^{232}$Th), and potassium-40 ($^{40}$K). Their decay releases energy in the form of alpha particles, electrons, geoneutrinos, and gamma radiation.

Approximately twenty percent of the released energy radiates into space unobstructed in the form of geoneutrinos (3–8 TW). The remaining energy heats up the planet (11–38 TW). The primordial heat flow contributes to 5–38 TW while 14–46 TW is being produced by radioactive decay (Dye, 2012). Different models for the Earth's total heat production are in poor agreement with each other, but in simplified terms approximately half of the total heat flow is contributed by primordial heat and radioactivity each.

The Earth's structure consists of five domains (Boehler, 1996; Figure 1): the inner core, outer core, lower mantle, upper mantle, and lithosphere. The core is metallic and consists of iron. The inner core is solid whereas the outer core is liquid. The mantle consists largely of magnesium silicate minerals and is ductile and locally partially molten. The lithosphere consists of silicate minerals and is solid. It is subdivided into the lower rigid lithospheric mantle and on top is the Earth's crust.

In the solid parts of the Earth **conductive heat transfer** occurs, whereas in liquid and ductile parts **convection** redistributes heat. In addition to these two processes, heat is redistributed by circulation of hot groundwater, primarily in the oceanic crust, and a small amount by advective heat transfer by the vertical movement of magma through the lithosphere. Since the lithosphere is solid and heat flow is mainly conductive, the thick lithosphere underneath the Earth's continents acts as a thermally insulating boundary between the convecting mantle and outer space.

The temperature difference between the Earth's core and surface is called the **geothermal gradient**, or geotherm, and is normally expressed in degrees Celsius per kilometre (°C/km). The geothermal gradient varies largely between the Earth's domains and on a small scale in the lithosphere depending on the local composition of the bedrock.

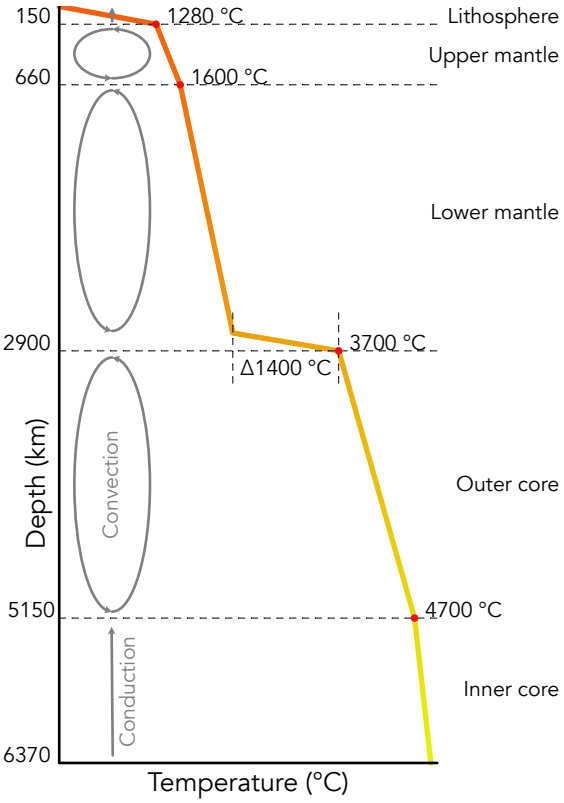


**Figure 1.** Schematic depth profile of the geothermal gradient from the core to the Earth's surface through different domains, characterised by different modes of heat transfer (Boehler, 1996).

Uranium, thorium, and potassium are radioactive chemical elements, which in geochemical classification belong to "lithophile" (rock-loving) elements (Goldschmidt, 1937). These elements bind to oxygen rather than to iron or sulphur and therefore occur in higher concentrations in the lithosphere than in the Earth's metallic core. The average concentrations of uranium, thorium, and potassium are higher in the Earth's crust than in the mantle, and the core is nearly entirely devoid of these elements (McDonough, 2003). The high concentrations of radioactive elements in the crust contribute with a substantial part of the Earth's total heat flow, despite of the crust being volumetrically subordinate to the mantle. The total heat flow through the crust consists therefore in part of heat from the Earth's interior passing through by conductive heat transfer, and in part by radiogenic heat produced within the crust.

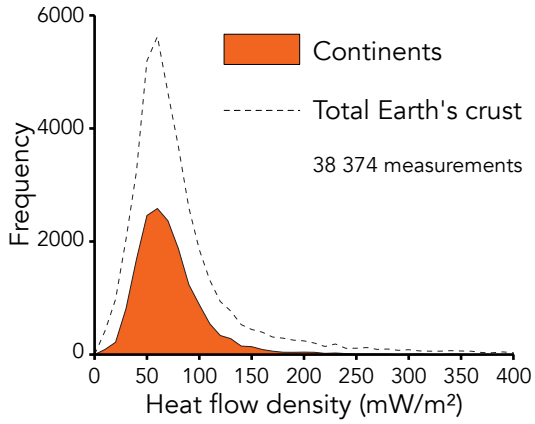


**Figure 2.** Heat flow density of the Earth's continental crust based on many measurements (modified from Davies & Davies, 2010).

Since the total heat flow through the Earth's surface is 43–49 TW (Dye, 2012), the global average heat flow per surface area (**heat flow density**) is approximately 91.6 mW/m², which can be subdivided into 105.4 mW/m² for young and thin oceanic crust (ocean floor) and 70.9 mW/m² for thick continental crust, based on many measurements (Davies & Davies, 2010; Figure 2).

Heat flow density is an expression of the amount of heat energy that passes through a square metre of bedrock per second. The value of heat flow density is estimated from measurements of the geothermal gradient and the bedrock's heat conductivity, for example by measuring the temperature in deep drillholes and thermal conductivity of rocks from the hole and nearby area. Heat flow density is thus not measured directly but calculated from the following equation:

$$Q = \lambda \frac{\delta T}{\delta z}$$

- $Q$ = heat flow density (mW/m²)
- $\lambda$ = heat conductivity (W/m°C)
- $\frac{\delta T}{\delta z}$ = geothermal gradient (°C/km)

The global average geothermal gradient in the upper parts of the Earth's continental crust, away from tectonic plate boundaries, is of the order of **~25 °C/km**. Near plate boundaries and in areas with volcanic activity, it can be significantly higher. For example, at the Hengill geothermal field in Iceland, the geothermal gradient in the upper 2 km of the crust is 150 °C/km (Foulger, 1995).

## 2.2 Disturbance of the geothermal gradient

The average temperature of the bedrock at the Earth's surface corresponds to the annual mean temperature for the local climate. Changes in air temperature can affect the temperature in the bedrock near the surface. Seasonal changes in atmospheric temperature give rise to annual swings in the temperature profile down to several tens of metres depth in the bedrock.

Climate change, crustal uplift with erosion, and subsidence with sedimentation can affect the geothermal gradient to greater depths. The change in geothermal gradient as a response to changing surface conditions depends on the change in surface temperature, the bedrock's thermal diffusivity, and the time since the change with an exponentially decreasing effect with depth. Thermal diffusivity is the relationship between heat conductivity and heat capacity.

During the past 2.6 million years of Earth's history, the global climate has been characterised by an **ice age** with cyclically reoccurring periods of glaciation and shorter interglacial warm periods in between. The latest glaciation occurred between 115 to 11.7 thousand years ago. Several times during the latest glaciation, a kilometre-thick ice sheet covered all of Scandinavia, like how Antarctica and Greenland look today.

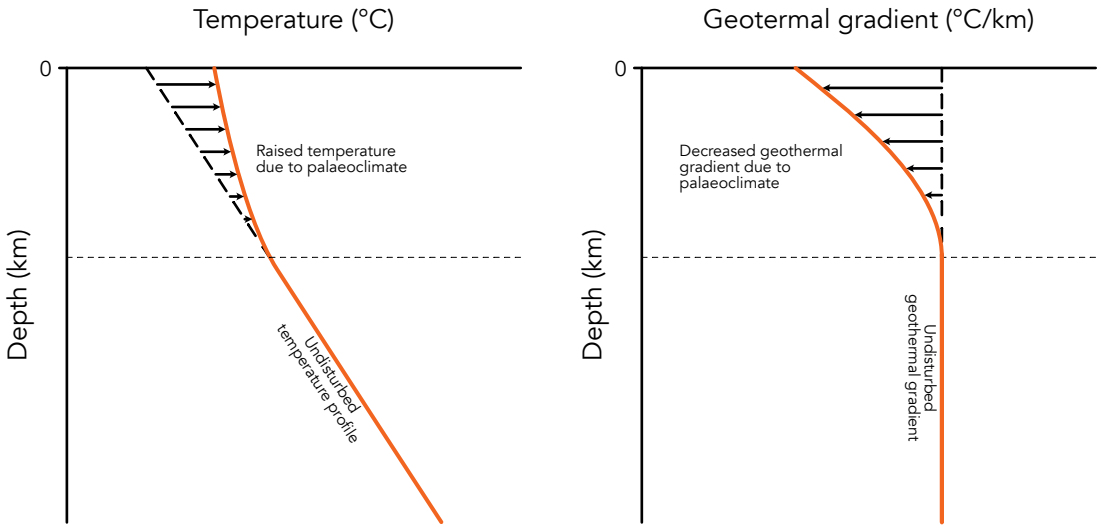


**Figure 3.** Schematic visualisation of the effect of a raised temperature in the upper part of the bedrock due to palaeoclimate and its influence on the geothermal gradient.

The Gothenburg area appeared from under the melting glacial ice approximately 16 thousand years ago (Larsen *et al.*, 2011). Since the climate in Gothenburg has been warmer for only a short period of a few thousand years after a longer period of glaciation, the bedrock has only heated up in response to this climate change near the surface. **Palaeoclimatic effects** have in Sweden and the Nordic region led to an increase in temperature but a corresponding decrease in geothermal gradient in the upper parts of the crust (Figure 3).

To determine the heat flow density with greater confidence, measurements of the geothermal gradient in relatively deep drillholes and modelling of the change in geothermal gradient are required. Modelling of the temperature disturbance due to climate change during the last 120 thousand years at Forsmark and Laxemar indicates that the geothermal gradient is disturbed down to at least 1 km depth (Sundberg *et al.*, 2009). The heat flow density in deep drillholes at Forsmark and Laxemar is calculated to be 36–37 mW/m² with the geothermal gradient at 200 m depth and 43–50 mW/m² using the gradient at 700–900 m depth. The corrected heat flow density, based on modelling of climate change during the last 120 thousand years, is estimated to be 56–59 mW/m²; an increase of approximately 20 mW/m². A similar palaeoclimate correction has been calculated on a regional scale by Balling (1995) and Majorowicz and Wybraniec (2011).

## 2.3 Enhanced Geothermal Systems

The search for geothermal heat available for extraction has historically focussed on natural geothermal systems, where natural hot fluids can be pumped up from hot reservoirs near the surface. These natural hydrothermal fluids can only be exploited for a limited amount of time, until the fluid is depleted. Another drawback is that such systems only occur in regions with exceptionally high heat flow, such as in volcanically active areas. To make geothermal energy more widely available, the concept was developed to artificially create hydrothermal reservoirs, which are called **Enhanced Geothermal Systems** (EGS). Investigations into EGS and the commercial extraction of deep geothermal energy began with the HDR research near Los Alamos in the United States in the early 1970s, which resulted in a successful EGS power plant with a thermal capacity of 10 MW (Olasolo *et al.*, 2016).

The general approach for EGS is to explore the Earth's crust for suitable areas where hot (relatively dry) rocks occur at depths of 4–5 km, where they potentially can be commercially exploited. Such areas are more common than natural hydrothermal reservoirs, which makes the prospect of geothermal energy extraction by EGS relevant for many more regions. The principal variable for the assessment is the geothermal gradient, since this determines the depth at which target temperatures are found. When a suitable volume of hot rock has been identified, wells are drilled into the rocks. By stimulating the rock volume, a permeable reservoir of fractures is created or enhanced, through which fluids can circulate.

Stimulation can be achieved in a variety of ways, of which the most common is so-called hydraulic stimulation. After drilling, the drillhole is closed off with an inflatable manchette at a certain depth. Large volumes of water

are pumped into the drillhole below the manchette, while at the same time monitoring the flow and pressure of the water. Water is injected into natural fractures and widens them so that the permeability increases. When the pressure is released, the fractures do not return to their original position and a permanent increase in permeability is achieved. Often, microseismic events are monitored during stimulation, which give a three-dimensional view of the location of the widened fractures around the drillhole, while also ensuring that regulated upper magnitudes of induced seismicity are not exceeded. Permeability can also be increased by so-called chemical stimulation, during which certain fracture-filling minerals can be dissolved by injecting acid. Other methods are explosive, jetting, and thermal stimulation.

An EGS power plant can operate as a closed system. Hot fluids are pumped up to a thermal or electrical power plant through production wells. Heat energy is extracted and the cooled fluid is injected back into the hot rock reservoir through an injection well. The fluid flows through permeable fractures and is heated up again. Some plants even use closed-loop binary cycle technology, in which the geothermal fluids do not directly power a turbine but rather heat up a second fluid that is used to generate electricity in a separate system.

## 2.4 Favourable geological conditions for EGS

Most deep geothermal projects in Europe are aiming to extract heat from naturally permeable layers of sedimentary rocks at depths of several kilometres. For example, many greenhouses in the Netherlands are transitioning from heating by burning natural gas to geothermal heat extracted from 2 km depth. In Sweden, thick layers of permeable sedimentary rocks at depths of several kilometres are mainly found near Gotland, Öland, and in southern Skåne. Therefore, this section focusses on favourable conditions for extraction of deep geothermal energy from **crystalline bedrock**, like the conditions in Gothenburg. Crystalline bedrock, or basement rocks, formed either from molten magma, such as granite, or recrystallised under conditions of high temperature and pressure to form gneiss.

There are multiple prominent deep geothermal projects in production or planning to extract geothermal energy from crystalline bedrock. Europe's first and still active EGS, Soultz-sous-Forêts in France, extracts geothermal heat energy from granitic bedrock through a system with three drillholes at 5 km depth and transforms the heat to electricity in a demonstration power plant with a capacity of 1.7 MWe. The bedrock consists of a 1.4 km thick upper layer of sedimentary rocks on top of fractured granite. At Rittershoffen, 6 km from Soulz-sous-Forêts, a heat power plant extracts 24 MWth heat energy through a system with two drillholes in the same granite, utilising a large zone of fractured bedrock at 2.5 km depth beneath a 2.2 km thick sedimentary cover. The United Downs Deep Geothermal Power project in Cornwall utilises a system with two drillholes to extract heat from a facture zone in granite at a depth of 5 km. The design of a binary power plant is currently being finalised and construction is planned to commence in 2023. The power plant is expected to deliver 1–3 MWe electrical capacity.

### 2.4.1 Heat production and radioactive granites

**Granite** is a relatively common rock type, which mainly consists of the minerals quartz and feldspar. Granite can form as a result of different geological processes and therefore there is a large variety in types of granite with different chemical compositions. Magma systems that produce granite are either characterised by long differentiation processes where granite forms among the final products of this process, or by processes in which other rocks are molten and where granite represents the first melt that is produced. In both scenarios, granite represents only a smaller volume that is produced from a larger volume of magma or partially molten bedrock.

Chemical elements like uranium, thorium, and potassium (with large ionic radii) have a strong affinity for granitic magma and can accumulate to high concentrations from a larger volume with lower concentrations. Since these three elements are naturally radioactive, granite is a rock type that generally has a higher content of radioactive elements than other rocks. Since natural radioactivity is a major source of heat in the Earth's crust, granite is in certain cases characterised by high heat production and thus by high heat flow density. For this reason, certain granitic bedrock, so-called "high heat flow granite", is often explored for geothermal energy.

Granite contains high concentrations of silica and has a high content of the mineral **quartz**. Quartz has a relatively high thermal conductivity compared to other silicate minerals. This means that a quartz-rich rock would show a lower geothermal gradient for the same heat flow density, compared to rocks with a lower content of quartz. Despite the higher thermal conductivity, granite is often a promising target in the exploration for geothermal energy, since the high radiogenic heat production in certain cases can wholly counteract the high content of quartz.

Previous research into the extraction of geothermal energy in Sweden has put a major emphasis on occurrences of granite with high concentrations of naturally radioactive elements, including the Bohus granite at Fjällbacka, Malingsbo granite in Bergslagen, and the Götemar granite near Oskarshamn.

### 2.4.2 Permeability and natural fracture zones

It is not enough to have hot bedrock with a high heat flow to extract geothermal energy, but it also requires a permeable reservoir. Water is used as carrier of the geothermal energy that is stored in the bedrock. For the water to extract heat efficiently from the hot rock, which has a relatively low thermal conductivity, an interface with a large surface area needs to exist in order to act like a heat exchanger.

Contrary to sedimentary bedrock, in which natural permeability may exist in pores between grains of sand, crystalline bedrock has very low natural permeability. The permeability in crystalline bedrock is entirely determined by the existence of **fractures**, their abundance, length, shape, direction, and surface coating by minerals.

Early investigations into the extraction of geothermal energy were driven by the idea to create a new permeable reservoir by hydraulic fracturing of the "hot dry rock". However, it was found that the hydraulic stimulation rather widened the existing natural fractures (Wallroth *et al.*, 1999). The modern concept of EGS is to stimulate natural fractures to increase the permeability of the bedrock.

Natural fracture zones are successfully exploited in the Upper Rhine Valley, including at Soultz-sous-Forêts and Rittershoffen in France and at Landau and Insheim in Germany. All these exploit reservoirs of naturally fractured granite, which after some degree of stimulation could be exploited for production of heat and electricity. The United Downs project will extract geothermal energy from a vertical natural fracture zone in granite. Earlier geothermal research in Sweden has also evaluated natural zones of permeability in the crystalline bedrock, including at lake Bullaren in Bohuslän and at the possible meteorite impact structure Björkö in Mälaren.

## 3. Local geological conditions and drill site location

### 3.1 Regional geology of the Gothenburg area

The Nordic bedrock largely consists of ancient, thick, and stable continental lithosphere, which is oldest (>2.5 billion years) in the northeast between Karelia and the Kola Peninsula, and which has successively grown toward the southwest. The bedrock in the Gothenburg area is part of what is referred to as the Southwest Swedish Gneiss Region ("Sydvästsvenska gnejsregionen"; Figure 4) and largely consists of varieties of crystalline gneiss and some granite.

The Southwest Swedish Gneiss Region has traditionally been divided into the Eastern and Western Segments. The rocks in the Eastern Segment formed approximately 1.7 billion years ago and comprise most of the bedrock south of lake Vänern, delimited to the east by a large north-south trending shear zone (Protogine Zone). The Eastern Segment consists of gneissic granitoids (rocks like granite; including tonalite, granodiorite, and granite), which have been affected by probably two continent-continent collisions. First at 1.4 billion years ago during the Hallandian and later by the Sveconorwegian mountain-building event between 1.1 and 0.9 billion years ago.

The rocks in the Western Segment (Figure 5) are younger and likely have a different geological origin than the Eastern Segment. The Western Segment formed during the Gothian mountain-building event at 1.7–1.5 billion years ago. The eastern part of the Western Segment, also called the Median Segment, mainly consists of gneissic granitoids that formed 1.6 billion years ago and are called the "A Group". The bedrock to the west of Göta Älv consists of a 1.6-billion-year-old belt of sedimentary gneiss, called the Stora Le–Marstrand Group, and younger gneissic granitoids that formed 1.56 billion years ago, which are called the "B Group". Approximately 1.3 billion years ago a long belt of diverse granites formed, which is mainly represented by the Askim and RA granites. The RA granite (**r**adio**a**ctive granite) received its name on account of the high concentrations of natural radioactive elements.

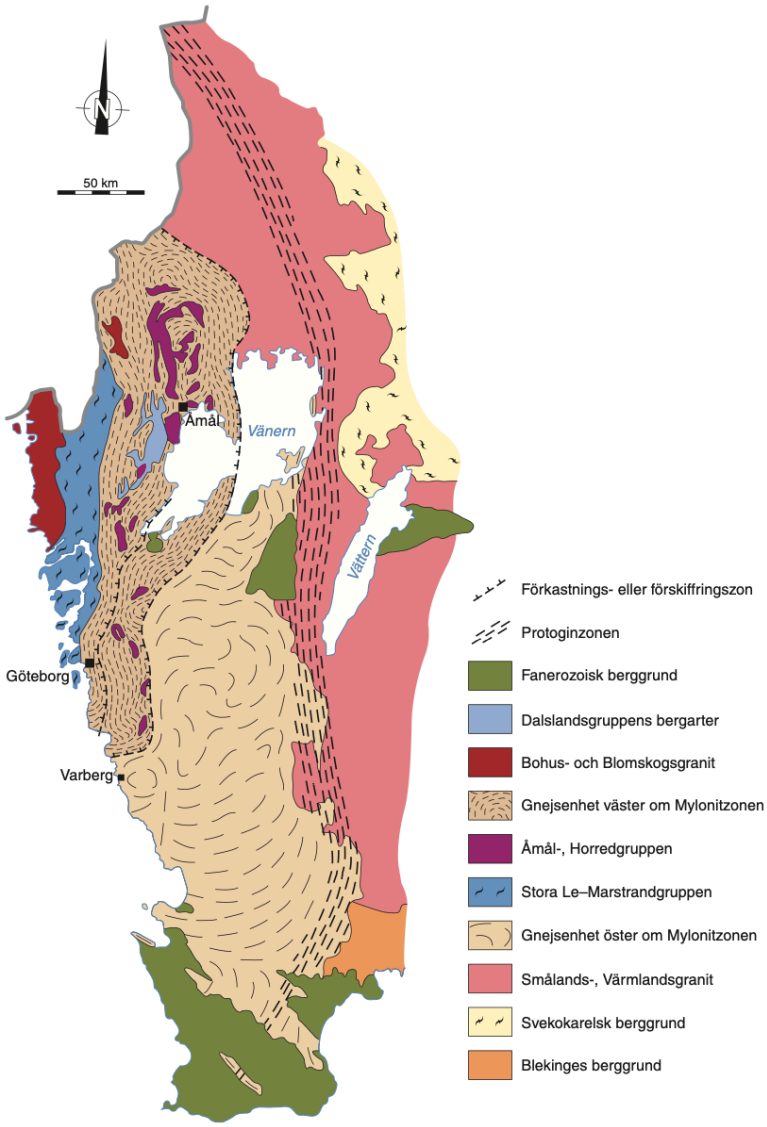


**Figure 4.** Regional bedrock map of the Southwest Swedish Gneiss Region. Source: Sveriges geologiska undersökning.

The bedrock in Gothenburg was also affected by the Sveconorwegian event. During mountain formation, the Western and Median Segments were thrust eastward on top of the Eastern Segment along a relatively shallowly dipping (15° to the west) north-south trending shear zone that is called the Mylonite Zone. Simultaneously, the Western Segment was likely thrust up on top of the Median Segment along a steeper zone (45–60° to the west) that is called the Göta Älv Zone, which largely coincides with the location of Göta Älv valley. During the late stages of the Sveconorwegian, the movement inverted and the segments slid back to some degree along the same zones.

In summary, the bedrock in Southwest Sweden has been shaped by **ancient mountains**, which have long since disappeared due to erosion. The rocks in the bedrock were shaped by these ancient processes and have remained in their current configuration since 1 billion years ago, when large-scale lateral and vertical movements of crustal segments took place along zones of weakness in the crust. The rocks in these zones are therefore rich in fractures. These fracture zones are more easily eroded than surrounding rocks and therefore they often coincide with valleys in the modern landscape. An understanding of these ancient processes can aid in explaining the modern-day structure and properties of the bedrock.

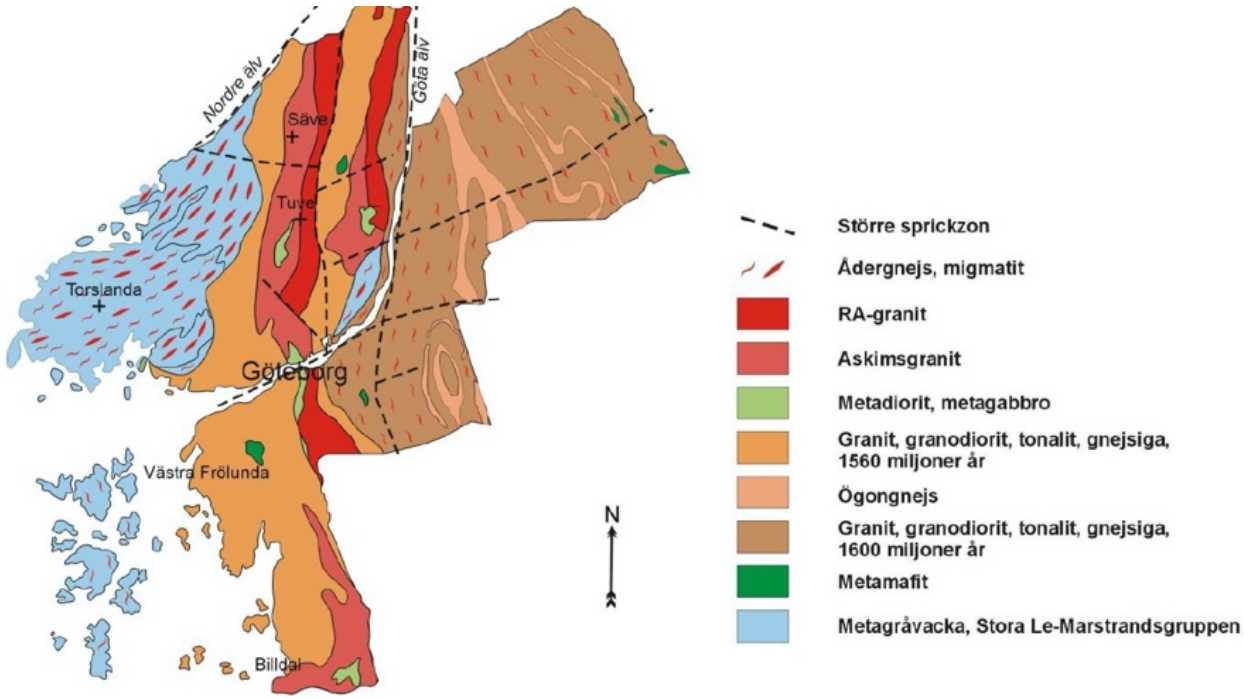


**Figure 5.** Simplified geological map of Gothenburg municipality. Source: Sveriges geologiska undersökning.

## 3.2 GE-2 drill site location

The two main favourable factors for extraction of geothermal energy from crystalline bedrock are: 1. radiogenic heat production, for example in granite, and 2. fracture zones with higher natural permeability. Based on simple modelling of the heat production and heat flow in rocks representing the different geological units in the Gothenburg area, the hypothesis was formed that the geothermal gradient could be highest in the RA granite due to the high radiogenic heat production (~7 μW/m$^3$). The drilling site of GE-1 was therefore chosen so that the drillhole would mainly pass through the RA granite, to test the area with the highest expected geothermal gradient. The result of the temperature measurements in GE-1 was a relatively low geothermal gradient of approximately 15 °C/km between 100 and 1000 m depth in the drillhole (Hogmalm *et al.*, 2021).

The site selection for GE-2 had the following aims: 1. to study the character of deep fractures in zones where the natural permeability in the bedrock is expected to be higher, and 2. to make a second measurement of the geothermal gradient.

The area between Västra Frölunda and Mölndal is characterised by low topographic relief. It coincides with a 40 km long E–W-trending series of valleys (lineament) from Hindås via Härryda, Landvetter, Mölnlycke, and Mölndal. This lineament is an erosional feature of the landscape, which is a likely topographic expression of a large fracture zone in the bedrock. East–west-trending fractures are common at the surface in Västra Frölunda, notable from Västra Frölunda church (Figure 6) and can be observed further south adjacent to road 159 (Figure 7) and south of the road.

**Figure 6.** Vertical fractures at Västra Frölunda church, view to the east.

**Figure 7.** Vertical fractures in the road cut south of Västra Frölunda church. View to the east from the bridge.

Scouting in this area selected the property Göteborg Kobbegården 151:2 as the best suited location for the drill site of GE-2. It is located south of road 159, in line with the fractures observed at Västra Frölunda (Figure 8). By drilling with a steep angle toward the northeast, perpendicular to the large-scale geological structures, the drillhole would be able to transect both the vertical E–W-trending fractures in the valley and potential fracture zones parallel to the main geological structure, like those encountered in GE-1.

The location of GE-2 to the southwest of GE-1 also has the benefit of being in the down-plunge direction of the RA granite, which was encountered from 172.47 m depth in GE-1. Since the general structures of the bedrock in this area dip to the west southwest, the RA granite could feasibly underlie the bedrock at GE-2 and potentially contributes with a higher heat flow to the B Group rocks above it.

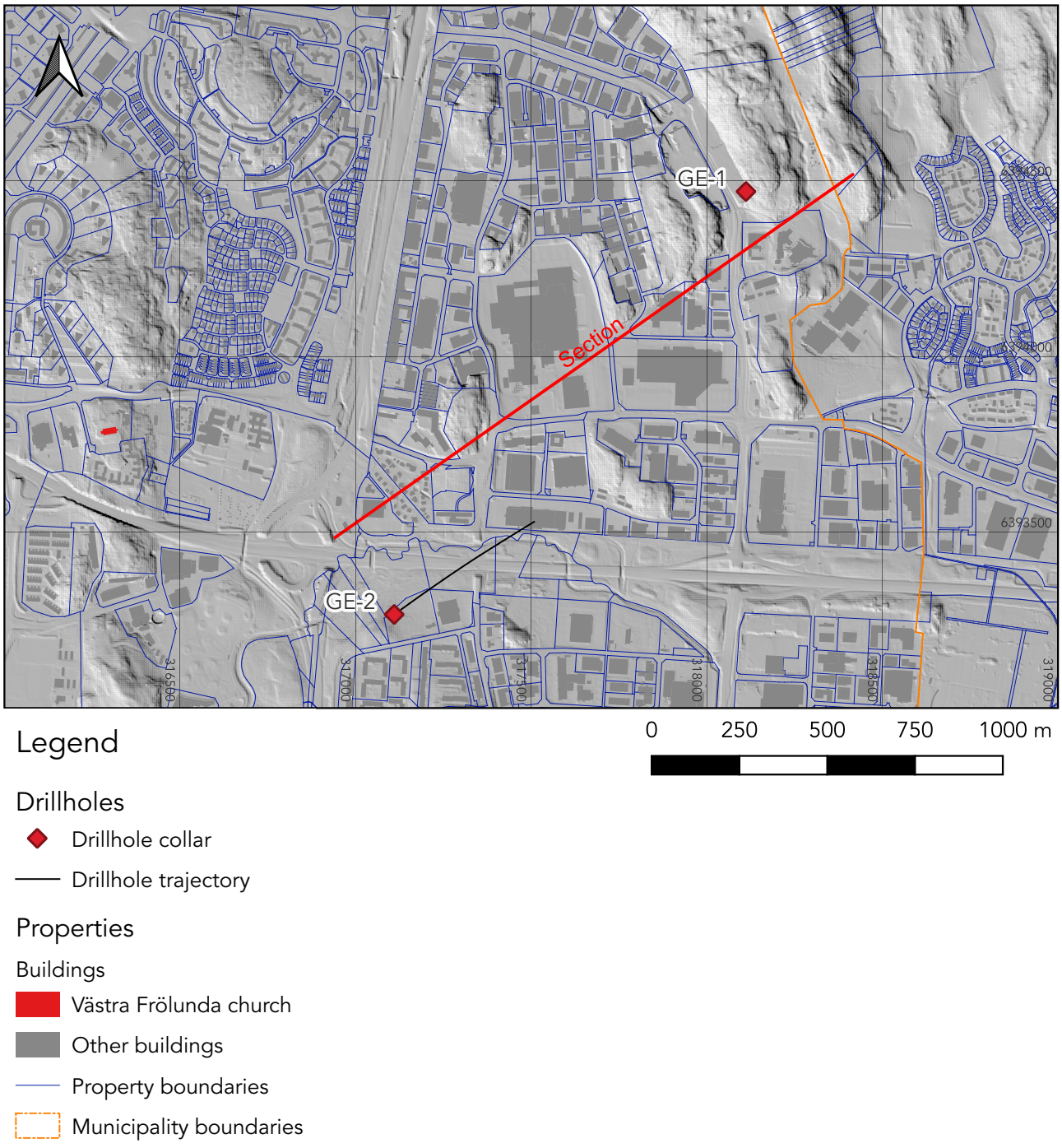


**Figure 8.** The location of GE-1 and GE-2 on an overview map of southern Gothenburg. East–west-trending vertical fractures occur at Västra Frölunda church (Figure 6) and further south in the road cut (Figure 7).

## 4. Drilling

Drilling was conducted by GEO-gruppen i Göteborg AB using an electrically powered Sandvik DE140 compact core drilling rig (Figure 9). The drillhole is located inside a large concrete ring, which captured drill cuttings from the hole and will protect the drillhole collar for future studies. A steel casing was drilled down into the bedrock surface and cemented in place.

Drilling water consisted of fresh water from the mains. Drill cuttings that washed out of the hole during drilling were pumped out of the concrete ring and collected in sedimentation tanks that consisted of two 20-ft. containers, each containing three compartments. The cleared water infiltrated into the ground. A sludge truck collected the drill cuttings from the sedimentation tanks.

The drillhole starting azimuth (direction) was 55° and the dip angle was 70°. The planned total depth was 1300 metres. The depth of overburden was 10.2 metres. The steel casing tube was drilled down to 11.45 metres. Standard wireline core drilling commenced with NQ2 (50.6 mm diameter) on 3 February 2022. Drill cores were extracted in runs of 6 m length.

**Figure 9.** Drill site of GE-2. Photo: David Nilsson.

The drillers noted clay at 123 metres depth on 8 February, corresponding to a zone of crushed rock. On 10 February, silt, sand, and gravel debris fell into the hole. Therefore, the drillers injected the hole with concrete to hopefully seal the fractures at 123 metres depth, after which they drilled out the concrete from the drillhole and continued. However, on the morning of 1 March, a 15-metre-tall column of drill cuttings had settled on top of the inner tube, despite thorough flushing of the hole with fresh water at the end of the previous shift. The conclusion was that water and drill cuttings, which had become pressurised during drilling, had leaked into the drill string during the night. The hole was therefore injected with concrete again, in a second attempt to seal the fractures. The issues with infiltrating drill cuttings ceased after the second round of concrete injection. Drilling continued without major obstacles, with some delays due to sick leave.

Following the drilling out of the injected concrete, the water in the sedimentation tanks became highly alkaline, showing pH values up to 13. The pH of the water in the tanks was neutralised by careful calculated addition of 30 % hydrochloric acid and thorough mixing of the water with the aid of an electric drill.

On 25 April the drillers transitioned to a smaller drill diameter (BQTK) at 745 metres depth. The drillers planned to finish the hole by telescope drilling inside the NQ2 drill string, however the water flow was too restricted inside the NQ rods. Therefore, they switched back to NQ2 on 2 May from 747 metres and continued with the same diameter despite the drilling rig struggling with the weight of the NQ2 drill string.

On 14 June, the drilling was aborted earlier than planned at a total depth of 986.65 metres. The reason for ending the hole was the apparently low frequency of fractures observed in the core. We judged that drilling deeper would not provide significantly more information, since the main zone of interest had been reached. Drilling of hole GE-2 was completed in 132 days (Figure 10).

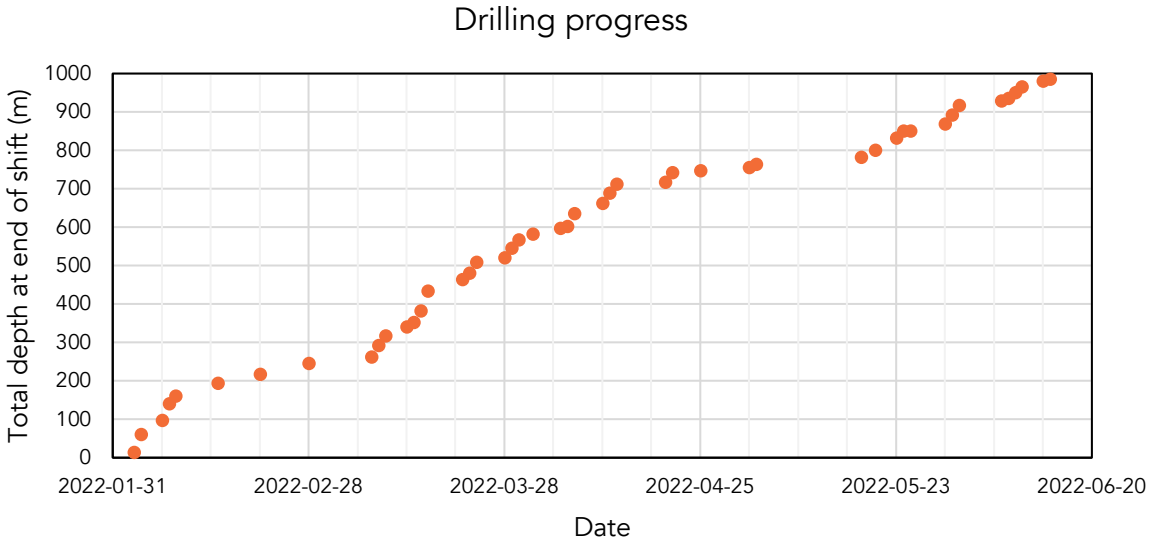


**Figure 10.** Drilling progress of GE-2 shown as the total depth of hole at the end of each shift.

Drillhole deviation was measured on two occasions by the drillers using a Devico DeviFlex survey tool, which is a non-magnetic in-rod measurement tool. Drillhole deviation surveys determine the actual direction of the drillhole, which normally deviates from the starting direction. Typical for diamond core drilling is that the drillhole trajectory gradually arcs to the right and lifts from the starting direction.

## 5. Drillhole logging

Staff from the Faculty of Engineering at Lund University (Lunds tekniska högskola) conducted two downhole surveys of the drillhole during 20 and 21 September 2022 (Figure 11), 98 days after drilling had finished. The first survey (ELTG) measured temperature, natural gamma radiation, self potential, and short, long, and single-point normal resistivity down to 983 metres. Data were saved with a 1 cm resolution. The second survey comprised acoustic drillhole imaging down to 980 metres.

**Figure 11.** Drillhole logging of GE-2 by staff from Lunds tekniska högskola on 20 September 2022.

## 5.1 Temperature

The drillhole temperature was recorded from a downhole depth of 15.11 metres (Figure 12). The survey tool output a temperature reading for every centimetre. The high-resolution temperature data are noisy and computationally heavy due to the large number of data points. Therefore, we first denoised and downscaled the data by calculating mean values for each metre, where the value for each downhole depth $x$ represents the mean of the interval from $x - 0.5$ to $x + 0.49$. For example, the value at depth 16 metres is the mean of the values recorded from 15.50 to 16.49 metres. To calculate the geothermal gradient, we converted the downhole depths to vertical depth below surface using the drillhole deviation survey data.

The temperature at 15 metres below surface is approximately 8.7 °C, which is close to the 1991–2020 average temperature in Gothenburg at 8.9 °C (data from SMHI, retrieved 29 November 2022). The maximum average drillhole temperature is 22.247 °C at 981 metres downhole, corresponding to a vertical depth of 856.7 metres below the surface. The geothermal gradient increases gradually from less than 5 °C/km near the surface to about 17 °C/km at 200 metres depth and remains relatively constant from there on. The geothermal gradient, calculated by simple linear regression of temperature data averaged over 1 metre intervals between 200 metres below surface and the bottom of hole, is 16.94 ± 0.02 °C/km (*SE*, $R^2 = 0.9989$, $n = 758$) with an intercept value of 7.64 °C at surface level. Using a calculated average thermal conductivity value for the B Group gneisses of 3.15 W/m°C, this results in an apparent (uncorrected) heat flow density of 53.4 mW/m$^2$.

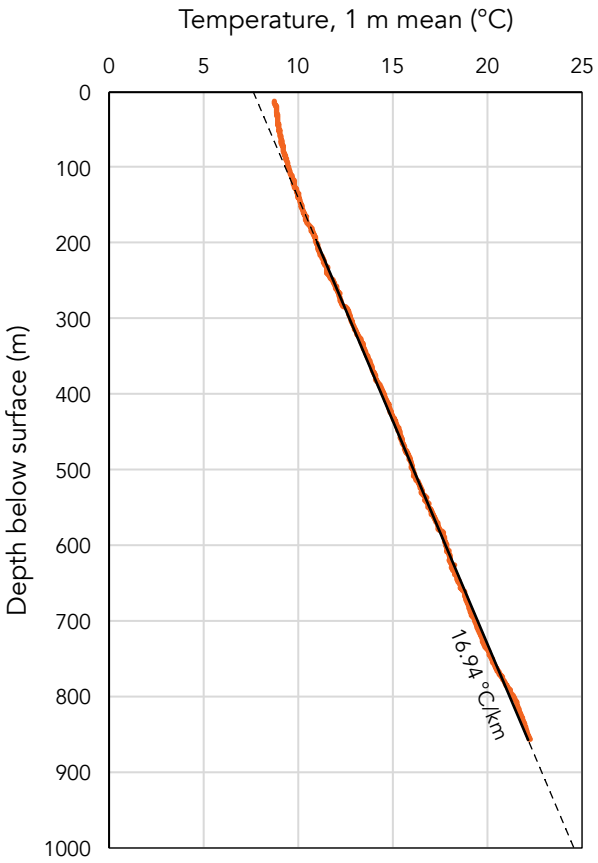


**Figure 12.** Drillhole temperature shown as a function of depth, corrected for drillhole deviation. The geothermal gradient below 200 metres depth is 16.94 °C/km.

## 6. Drill core logging

Drill core logging was conducted by staff from Axray Scientific AB. Drill core boxes were inspected and collected from site regularly during drilling. Detailed drill core logging took place mainly during October–December 2022 and comprised ocular rock descriptions and characterisation of planar structures, such as veins, foliation, and natural fractures in the drill core, including the depth, angle to the core axis, roughness, alteration, thickness, and minerals on fracture surfaces. Data were recorded in a digital spreadsheet. Digital colour photographs of dry and wet drill core were taken.

### 6.1 Lithology

The lithology (description of rock units; Figure 13) was determined through optical inspection with terminology according to the igneous and metamorphic rock classification schemes of the International Union of Geological Sciences (Le Maitre, ed., 2002; Schmid *et al.*, 2007). In order to distinguish the gneiss lithologies from each other, protolith-indicating prefixes from the igneous rock classification QAPF diagram were applied to the gneiss lithologies. The classification is based on visual mineral and textural characteristics. In addition, natural gamma radiation intensity values have been used to distinguish distinct granite generations (Figure 13).

The granitic, granodioritic, and tonalitic gneisses that occur from the surface down to 911 m core depth probably belong to the B Group. The composition and deformation intensity of the B Group gneisses vary throughout the core, including shifts between porphyritic, lensoidal, and banded textures in medium to coarse grain sizes. The rocks locally display folding structures.

Red-staining from iron-rich microcrystals, and possibly associated modification of feldspar minerals, has affected the gneisses. Feldspar alteration may obscure the ocular distinction between K-feldspar and plagioclase, thereby limiting the ability to interpret the precursor magmatic rocks of the gneisses by visual appearance in the absence of microscopic and chemical investigations. Pegmatitic quartz-dominated veins occur throughout the core. Epidote and chlorite alterations occur occasionally.

At a depth of 911 m, the natural gamma radiation intensity median value increases from 125 cps (above 895 m) to 563 cps (Figure 13). This increase in natural radioactivity indicates the upper contact to the 1.3-billion-year-old RA granite. Furthermore, its homogeneous granitic composition and the occurrence of accessory magnetite crystals are in line with observations of RA granite in GE-1 (Hogmalm *et al.*, 2021).

## 6.2 Fractures

A total of 1277 natural fractures were identified during drill core logging of GE-2. Of these, 703 (55 %) are in the upper 500 m of the drill core. A total of 903 open fractures were also recognised in the acoustic drillhole imaging data. In GE-1, acoustic imaging recognised 450 open fractures, as compared to 717 fractures identified during drill core logging of GE-1. Most of the fractures that are not visible in the acoustic imaging data sit along biotite- and chlorite-rich foliation planes, where fracturing may not have fully developed until the drilling operation reopened previously at least partially sealed fractures. Many of the foliation plane fractures are especially susceptible to slip, given their smooth surfaces (low joint roughness values) and mica-rich coatings, and as demonstrated by their frequent opening by the drilling procedure. Although not completely open and highly permeable in their steady state, the sealed and partially sealed fractures still constitute inherent rock weaknesses and may therefore become more permeable after stimulation.

Fracture frequencies have been evaluated in intervals of 5 metres (Figure 13). The fractures cluster in zones with high fracture frequency in the uppermost 150 m of the drill core, including a maximum of 53 fractures identified within the 75–80 m interval and 54 fractures within the 120–125 m interval. A section of relative fracture scarcity follows between 150 m and 300 m depth (58 fractures) before an intensified fracturing section at 300–350 m (126 fractures). Fracture frequencies are more uniform below the 350 m level, where fracture-rich sections do not exceed 20 fractures per 5 m interval except for the 850–855 m interval with 51 fractures.

A total of 32 sections do not contain any fractures in the 5-metre interval. The longest coherent section without fractures is 25.5 m long. The collective lengths of these 32 intervals add up to 284.1 m, corresponding to 29 % of the total drill core length. In total, GE-2 has a higher apparent fracture frequency compared to GE-1, which contained 48 sections without fractures in the 5 m intervals, corresponding to 52 % of the total core length. Fracture frequencies in GE-1 do not exceed 30 per 5 m interval.

Fracture distribution within GE-2 is not directly controlled by lithology as the rock types that host the highest fracture frequencies vary. The abundant fracture sets between 70–130 m and 342–350 m are mainly hosted in moderately deformed, occasionally porphyritic granitic gneiss, whereas strongly deformed biotite-rich granodioritic to tonalitic gneiss hosts the intensified fracturing rates between 140–145 m and 304–320 m.

The fractures in intensely fractured sections are typically parallel to the foliation direction of deformed rocks with abundant biotite- and chlorite-rich foliation bands. The fracture rate has likely been enhanced in these zones by the high slip susceptibility of often smooth chlorite- and biotite-coated foliation planes. The severely fractured section at 851–853 m in the strongly deformed and chlorite- and biotite-altered contact between an occasionally porphyritic granodioritic gneiss and a finer grained biotite-rich tonalitic gneiss is the most prominent example of this fracturing style. The enhanced fracture rate is controlled by zones of strong deformation and coeval fluid circulation causing extensive chlorite alteration along foliation planes. This style of fracturing also dominates in zones with the highest fracture frequencies in GE-1 (at 400–420, 580–600, and 900–910 m), there mainly associated with intensely deformed metabasite rocks.

In contrast, the fracture-rich zones located in less deformed rocks of various compositions comprise fracture sets that crosscut the foliation, which contain calcite, quartz, and pyrite as common fracture coating minerals. This fracturing style is more frequently observed in GE-2 than in GE-1. Rather than reflecting a difference in fracture occurrences, this may also be explained by the vertical orientation of GE-1, which is much less likely to intersect subvertical fractures than the 70° angled orientation of GE-2.

A total of 23 open fractures in GE-2 displays a significantly larger aperture relative to the rest in the acoustic image. All occur in the upper 367 m of the drillhole.

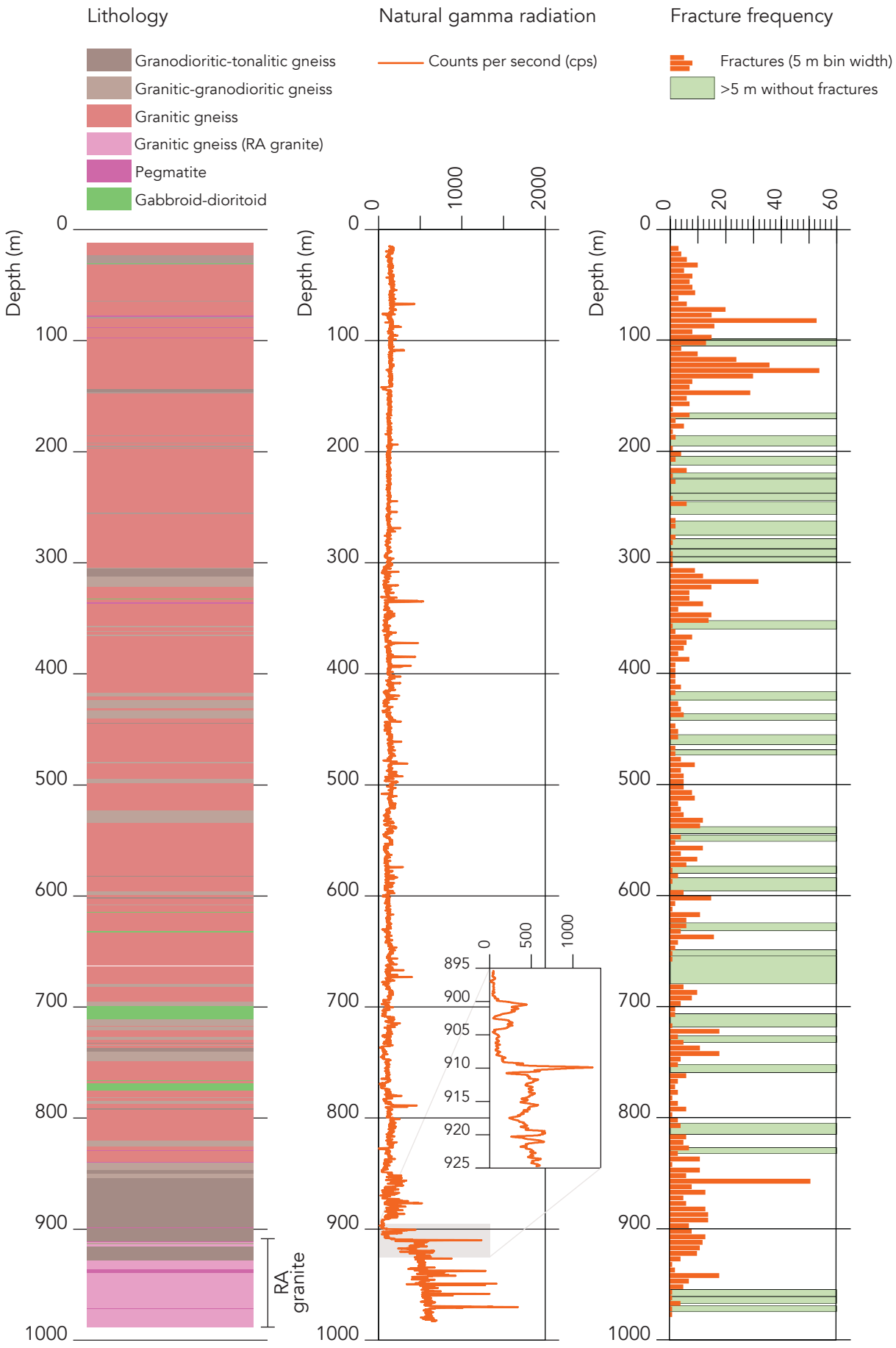


**Figure 13.** Lithology log of the GE-2 drill core, highlighting the transition in natural gamma radiation coincident with RA granite. The binned 5-metre fracture frequency reflects zones of weak and intense fracturing in the core.

## 6.3 Fracture set analysis

The dip angles and dip directions of fractures were derived from the acoustic drillhole imaging data. Only completely open fractures, which are visible on the acoustic image, are included and the recorded dip and dip direction data are paired for each specific fracture. Apparent dip directions of fracture ellipses were read straight off the acoustic images. Trigonometric calculations of acoustic imaging data measured on millimetre scale provided apparent dip angles. These readings transform to true dip angle and dip directions using a set of equations developed by Stanley and Hooper (2003) by also considering the drillhole deviation. We used Rick Allmendinger's Stereonet 11 software to plot the data in stereographic projection on stereonets including density contours of poles to fracture planes.

The discrepancy between the fracture abundance observed during logging of the drill core and the lower number of open fractures detected in the acoustic images is not evenly distributed throughout the drillhole depth (Figure 14). In short, the logged drill core fractures are more abundant in most depth intervals, a trend especially pronounced in the 50–150 m interval. This could be explained by the two rounds of concrete injection in the uppermost part of the drillhole, which sealed open fractures in the drillhole wall.

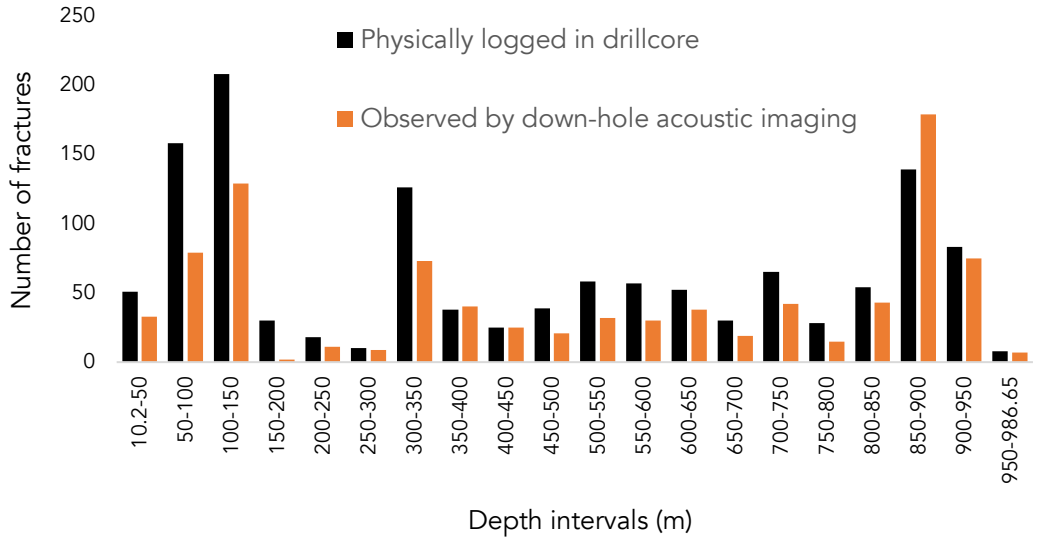


**Figure 14.** Number of fractures recorded by observations of the drill core and acoustic drillhole imaging data in 50-metre intervals.

The acoustic images show slightly higher fracture frequency than observed in the drill core between 350–400 m and much higher between 850–900 m. These fractures have fresh and unmineralised surfaces in the drill core and are often located along foliation planes and were therefore classified as drilling induced fractures. The discrepancy between the fracture abundance recorded by drill core logging and acoustic imaging does not affect the fracture set analysis more than a relative emphasis of fracture abundance within fracture sets common within the 350–400 m and 850–900 m sections compared to the other sections.

The uncertainty of measured dip angles and dip directions for individual fractures is likely at least ±10° for both sets of values as a result of fracture plane irregularity and the accuracy of acoustic image readings. The relatively short intersection of the drillhole through an undulating fracture plane results in substantial uncertainty in angles of individual fractures to begin with. Therefore, we judge that the precision of the measured dip angles and dip directions is fit for purpose.

Dip angles were frequently underestimated from the acoustic image. The actual fracture sets are thus likely steeper than these data suggest, not seldom in the order of >10° for less steeply dipping beds, based on correlation with measurements of fractures in the drill core where possible. The use of oriented drill core would have obtained more accurate dip angles and dip directions of fractures, but the acoustic imaging data analysis nonetheless allows a consistent estimation of fracture set groupings.

Dividing the fractures into dip direction bins of 10°, fractures occur in all intervals (Figure 15). Fractures dipping to between 160 and 250° from N (dip to SSE to WSW) are by far most abundant. Frequencies higher than 20 fractures per 10° interval occur between 60–70° (dip to ENE) and between 350–10° (dip to N).

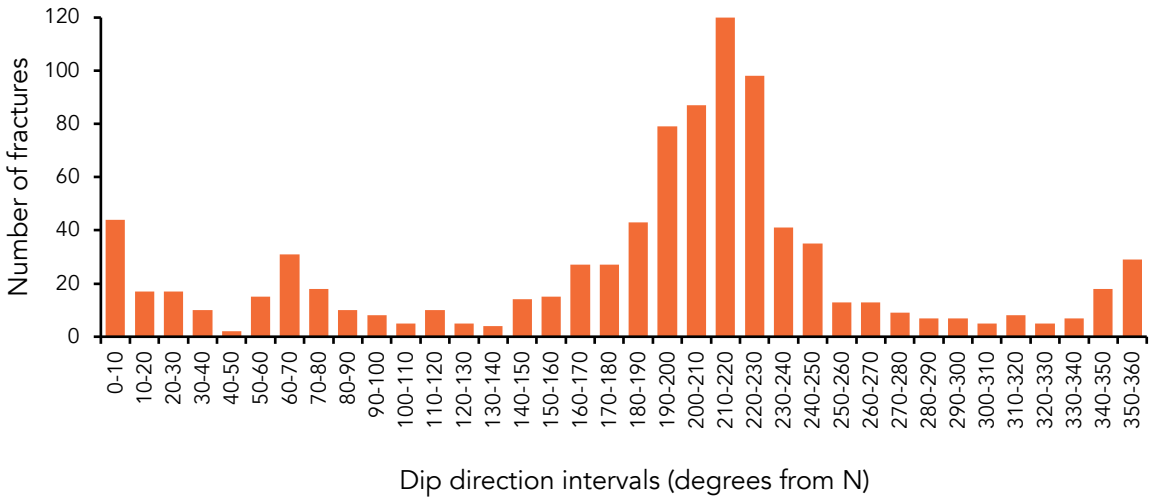


**Figure 15.** Fracture frequency in 10° dip direction intervals.

The combined analysis of dip angle and dip direction on a stereonet (Figure 16) and matrices (Table 1) distinguishes three or four predominant fracture sets. The most abundant fracture set occurs as SE–NW-trending (130–310° on average) fractures that dip to the SW (220° dip direction) with an estimated dip angle of 40°. An extensive number of fractures belongs to a nearly identical set with an ESE–WNW (122–302°) trend at a slightly steeper (45°) dip angle to the SSW (212°), but it is possible that this peak in fracture frequency is the result of the data collection method.

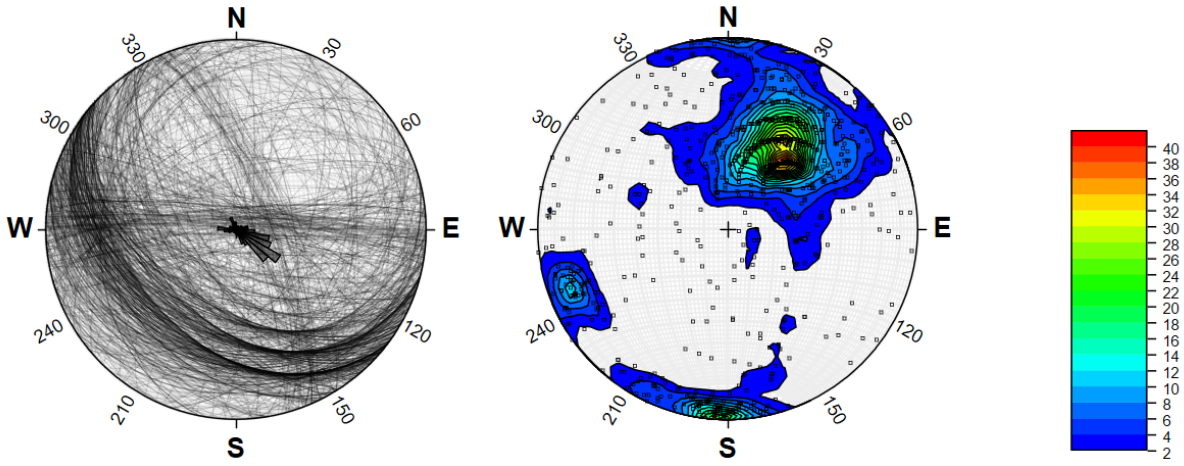


**Figure 16.** Stereographic projection of all fracture dip angles and dip directions as half-circles and with strike angles indicated in the central rose diagram (left), and corresponding poles to fracture planes and smoothed kamb density contours (indicating number of fractures) using a grid node number of 40 and a significance level of 3 (right).

Both fracture sets have biotite- and chlorite-coated surfaces, occasionally with sporadic calcite, illite, K-feldspar, and epidote, and typically extend along foliation planes. The correlation with foliation is emphasised in the depth-sorted data, where some of the most intensely foliated and biotite- and chlorite-rich rock sections at 850–900 m coincide with the highest fracture frequency of the SW-dipping fracture set. The foliation orientation has not been recorded in the absence of drill core orientation, but the correlation between the SW-dipping fracture sets and foliation is overall strong. The dip angle and dip direction of these fracture sets may therefore serve as a rough indicator of the foliation. However, the foliation and fracture trends were complex in the GE-1 drill core (Ladefoged, 2021), which thus makes such predictions precarious.

Two additional, less frequent and more steeply dipping fracture sets are distinguished. The first set is almost vertical (88°) and trends E–W (93–273°), on average dipping slightly to N (3°). This fracture set is notably most common between 400–700 m depth (Table 1), often appearing in batches of 2–5 fractures with a downhole spacing a few decimetres. The fractures are typically rough and almost exclusively coated by calcite. Another set

is NNW–SSE-trending (340–160°) and dips 78° to the ENE. This set is more evenly distributed in four sections (10–100 m, 300–400 m, 500–600 m, and 700–800 m). Calcite is the most frequently encountered mineral coating, followed by chlorite as second most common and only sporadic quartz, illite, K-feldspar, and epidote. Fractures without mineral coating are also present.

**Table 1.** Matrices showing the frequencies of fracture dip direction in 10° divisions compared to depth (left) and fracture dip angle (right).

Dow n-hole depth intervals (m)

| Dip direction intervals (degrees) | 10.2-100 | 100-200 | 200-300 | 300-400 | 400-500 | 500-600 | 600-700 | 700-800 | 800-900 | 900-986.86 |
|---|---|---|---|---|---|---|---|---|---|---|
| 0-10 | 2 | 1 | 1 | 2 | 12 | 11 | 11 | 2 | 2 | 0 |
| 10-20 | 0 | 2 | 2 | 0 | 2 | 3 | 5 | 3 | 0 | 0 |
| 20-30 | 1 | 1 | 0 | 0 | 2 | 0 | 5 | 0 | 1 | 7 |
| 30-40 | 0 | 1 | 0 | 2 | 0 | 0 | 0 | 0 | 0 | 7 |
| 40-50 | 0 | 0 | 0 | 0 | 0 | 0 | 0 | 0 | 0 | 2 |
| 50-60 | 4 | 4 | 0 | 1 | 0 | 0 | 0 | 4 | 2 | 0 |
| 60-70 | 6 | 1 | 2 | 6 | 0 | 8 | 0 | 7 | 0 | 1 |
| 70-80 | 2 | 0 | 1 | 4 | 3 | 1 | 2 | 3 | 1 | 1 |
| 80-90 | 1 | 3 | 0 | 3 | 0 | 1 | 0 | 0 | 0 | 2 |
| 90-100 | 1 | 4 | 1 | 1 | 0 | 0 | 0 | 1 | 0 | 0 |
| 100-110 | 2 | 1 | 0 | 1 | 0 | 0 | 0 | 0 | 0 | 1 |
| 110-120 | 4 | 4 | 0 | 0 | 0 | 0 | 1 | 0 | 0 | 1 |
| 120-130 | 2 | 1 | 0 | 0 | 0 | 0 | 1 | 0 | 1 | 0 |
| 130-140 | 0 | 3 | 0 | 0 | 0 | 0 | 0 | 0 | 1 | 0 |
| 140-150 | 2 | 9 | 0 | 2 | 0 | 0 | 0 | 0 | 0 | 1 |
| 150-160 | 1 | 4 | 0 | 1 | 0 | 5 | 1 | 0 | 0 | 3 |
| 160-170 | 3 | 7 | 0 | 3 | 2 | 2 | 3 | 0 | 2 | 5 |
| 170-180 | 5 | 9 | 0 | 2 | 2 | 1 | 3 | 0 | 2 | 3 |
| 180-190 | 7 | 9 | 0 | 8 | 5 | 4 | 5 | 0 | 1 | 4 |
| 190-200 | 3 | 5 | 0 | 17 | 3 | 1 | 5 | 1 | 28 | 16 |
| 200-210 | 8 | 9 | 1 | 25 | 2 | 0 | 5 | 2 | 30 | 5 |
| 210-220 | 11 | 14 | 1 | 14 | 1 | 4 | 2 | 4 | 58 | 11 |
| 220-230 | 4 | 6 | 0 | 4 | 1 | 1 | 0 | 7 | 69 | 6 |
| 230-240 | 9 | 3 | 0 | 2 | 1 | 0 | 3 | 9 | 12 | 2 |
| 240-250 | 7 | 6 | 1 | 2 | 1 | 5 | 2 | 8 | 3 | 1 |
| 250-260 | 3 | 5 | 1 | 0 | 0 | 1 | 0 | 1 | 2 | 0 |
| 260-270 | 4 | 4 | 0 | 0 | 0 | 0 | 0 | 3 | 2 | 0 |
| 270-280 | 4 | 2 | 0 | 1 | 0 | 0 | 0 | 1 | 0 | 1 |
| 280-290 | 3 | 0 | 2 | 1 | 0 | 0 | 0 | 0 | 1 | 0 |
| 290-300 | 4 | 2 | 0 | 0 | 0 | 0 | 0 | 0 | 0 | 1 |
| 300-310 | 2 | 2 | 0 | 0 | 0 | 1 | 0 | 0 | 0 | 0 |
| 310-320 | 1 | 2 | 1 | 1 | 1 | 1 | 0 | 0 | 0 | 1 |
| 320-330 | 3 | 2 | 0 | 0 | 0 | 0 | 0 | 0 | 0 | 0 |
| 330-340 | 2 | 3 | 0 | 0 | 0 | 0 | 1 | 0 | 1 | 0 |
| 340-350 | 1 | 1 | 4 | 5 | 1 | 5 | 0 | 1 | 0 | 0 |
| 350-360 | 1 | 1 | 2 | 5 | 8 | 7 | 2 | 0 | 3 | 0 |

Legend: >4 >9 number of fractures

Dip angle intervals (degrees)

| Dip direction intervals (degrees) | 0-10 | 10-20 | 20-30 | 30-40 | 40-50 | 50-60 | 60-70 | 70-80 | 80-90 |
|---|---|---|---|---|---|---|---|---|---|
| 0-10 | 0 | 0 | 1 | 1 | 0 | 1 | 0 | 3 | 38 |
| 10-20 | 0 | 0 | 1 | 0 | 1 | 2 | 0 | 5 | 8 |
| 20-30 | 0 | 0 | 0 | 0 | 1 | 0 | 0 | 7 | 9 |
| 30-40 | 0 | 1 | 0 | 1 | 0 | 0 | 0 | 3 | 5 |
| 40-50 | 0 | 0 | 0 | 0 | 0 | 0 | 1 | 0 | 1 |
| 50-60 | 0 | 1 | 1 | 1 | 0 | 1 | 6 | 1 | 4 |
| 60-70 | 0 | 1 | 1 | 0 | 2 | 0 | 7 | 13 | 7 |
| 70-80 | 0 | 0 | 0 | 1 | 0 | 0 | 3 | 11 | 3 |
| 80-90 | 0 | 0 | 1 | 2 | 0 | 1 | 2 | 1 | 3 |
| 90-100 | 0 | 0 | 1 | 2 | 0 | 1 | 0 | 2 | 2 |
| 100-110 | 0 | 0 | 0 | 1 | 0 | 2 | 0 | 0 | 2 |
| 110-120 | 0 | 0 | 1 | 1 | 4 | 0 | 2 | 1 | 1 |
| 120-130 | 0 | 1 | 1 | 0 | 0 | 1 | 1 | 0 | 1 |
| 130-140 | 0 | 0 | 1 | 0 | 1 | 1 | 0 | 0 | 1 |
| 140-150 | 0 | 0 | 2 | 3 | 2 | 4 | 1 | 1 | 1 |
| 150-160 | 0 | 0 | 1 | 3 | 3 | 0 | 3 | 2 | 3 |
| 160-170 | 0 | 6 | 4 | 2 | 2 | 2 | 1 | 2 | 8 |
| 170-180 | 0 | 2 | 4 | 8 | 2 | 1 | 3 | 1 | 6 |
| 180-190 | 0 | 0 | 5 | 4 | 9 | 7 | 1 | 5 | 12 |
| 190-200 | 0 | 1 | 17 | 21 | 11 | 8 | 8 | 8 | 5 |
| 200-210 | 0 | 1 | 2 | 7 | 27 | 28 | 11 | 9 | 2 |
| 210-220 | 0 | 2 | 13 | 39 | 35 | 19 | 8 | 4 | 0 |
| 220-230 | 0 | 1 | 3 | 32 | 23 | 23 | 9 | 1 | 6 |
| 230-240 | 0 | 0 | 2 | 7 | 7 | 5 | 9 | 9 | 2 |
| 240-250 | 0 | 0 | 1 | 4 | 8 | 10 | 6 | 4 | 2 |
| 250-260 | 0 | 0 | 4 | 3 | 0 | 2 | 1 | 2 | 1 |
| 260-270 | 1 | 0 | 1 | 2 | 3 | 2 | 2 | 0 | 2 |
| 270-280 | 0 | 1 | 0 | 3 | 1 | 0 | 1 | 2 | 1 |
| 280-290 | 1 | 0 | 0 | 4 | 2 | 0 | 0 | 0 | 0 |
| 290-300 | 0 | 2 | 0 | 3 | 0 | 0 | 0 | 0 | 2 |
| 300-310 | 0 | 0 | 1 | 0 | 0 | 0 | 2 | 0 | 2 |
| 310-320 | 0 | 2 | 0 | 1 | 0 | 2 | 2 | 0 | 1 |
| 320-330 | 0 | 1 | 0 | 1 | 3 | 0 | 0 | 0 | 0 |
| 330-340 | 0 | 1 | 1 | 1 | 0 | 3 | 1 | 0 | 0 |
| 340-350 | 0 | 1 | 0 | 0 | 2 | 2 | 4 | 2 | 7 |
| 350-360 | 0 | 0 | 1 | 1 | 1 | 1 | 3 | 3 | 19 |

Legend: >4 >9 number of fractures

## 7. Discussion

### 7.1 Fracture sets and natural permeability

At least 903 open fractures occur along the total length of GE-2. The different fracture sets are inhomogeneously distributed along the length of the drillhole. There are zones of higher fracture frequency and zones with relative fracture scarcity (Figure 13). Most fractures in GE-2 belong to the SW–SSW-dipping biotite- and chlorite-rich fracture sets that are typically parallel to foliation planes. The mineral coatings with biotite and chlorite enable slipping. Therefore, these fractures are deemed more likely to respond to hydraulic stimulation than the subordinate and typically rougher N- and ENE-dipping fracture sets. Since GE-2 was drilled approximately perpendicular to the regional foliation in the gneisses, it is not unexpected that these fractures are most frequently intersected in the drillhole.

Approximately 73 fractures belong to the nearly vertical E–W-trending fracture set, which is likely the same as the fractures observed near Västra Frölunda church (Figures 6 and 7). This fracture set was of prime interest for the drilling of GE-2, since it is aligned with a major E–W-trending lineament in the landscape with presumed higher fracture frequency. Because GE-2 was drilled at a 70° angle to the ENE (55°), the apparent frequency of E–W-trending fractures in the drillhole is low. The N–S extent of GE-2, perpendicular to the E–W-trending fractures, is approximately 250 m (Figure 8). Since these fractures occur mainly between 300 and 700 m downhole depth (Table 1), they are constrained to a N–S extent of approximately 100 m. Therefore, the average spacing perpendicular to the fracture orientation is roughly 1.4 m.

During planning of GE-2, one of the working hypotheses was that the natural permeability (in essence, fracture frequency) would be amplified at the intersections between the E–W-trending vertical fractures and the fracture set parallel to the foliation. Although the hydraulic properties of these fracture sets have not been tested, the observations of these fracture sets in GE-2 do not obviously support the idea that these intersections are zones with exceptional natural permeability.

There is a general decrease in apparent fracture frequency with depth. The extensively fractured zone at 850–910 m depth is the only fracture zone in the lower half of the drillhole. Significantly, the fractures with substantial aperture, and thus high hydraulic permeability, all occur in the upper 367 m. The predictability of fracture frequency with depth is low due to the variability in distribution and frequency, the low fracture propagation frequency from surface towards depth, and due to that the distribution of zones of higher fracture frequency is not intimately controlled by lithology.

Although the distribution of fractures along the drillhole is highly variable, the number of fracture sets and their planar attitudes are clearly constrained and definable from the obtained data. This contrasts with the strongly varying directions and angles for both fractures and foliation in GE-1, at least in the upper 500 m (Ladefoged, 2021). The fracture dip directions and angles are more uniform with a main SW dip direction in the lower part of GE-1 as well as in outcrops in Änggårdsbergen (Lindell, 2022).

The other fracture sets identified in GE-2 are harder to project to GE-1. Due to the vertical orientation of the GE-1 drillhole, the nearly vertical E–W-trending fracture set does not necessarily intersect the GE-1 drillhole at all. The ENE-dipping set is observed in outcrop near GE-1 (Lindell, 2022) with a shallower average dip angle of 55° compared to 78° in GE-2. This fracture set is likely the conjugate set to the main set of SW–SSW-dipping fractures, which are parallel to the foliation in the gneissic rocks.

## 7.2 Geothermal gradient and heat flow density

Hogmalm *et al.* (2021) concluded that the geothermal gradient in GE-1 was approximately 15 °C/km below 100 metres. Using the same methodology as for GE-2, the geothermal gradient can indeed be estimated at 15.46 °C for the temperature from 100 metres depth and below.

A comparison of the temperature profiles of GE-1 and GE-2 leads to the following observations (Figure 17). The temperature is very different in the uppermost 100 metres. The temperatures are broadly equivalent at depths between 100 and 500 metres at approximately 17 °C/km. Below 500 metres, the geothermal gradient in GE-1 starts to diverge from this trend toward lower temperatures following a lower geothermal gradient of approximately 14.66 °C/km.

Differences in the upper 100 metres are potentially an expression of different affinity for seasonal variations. For example, there is a lot of exposed bedrock around GE-1, which perhaps could absorb solar irradiation and summer temperatures more effectively than the sediments that cover the bedrock surrounding GE-2.

The decrease in geothermal gradient in lower parts of GE-1 perhaps can be explained by that the remaining thickness of underlying heat-producing RA granite naturally decreases with depth, thus leading to a lower heat flow density in deeper parts of the RA granite body than near the top. In addition, the upper part of the RA granite seems to be more radioactive than lower parts (Figure 18), which therefore also leads to a decreasing heat production with depth. Since the RA granite is rich in the mineral quartz, it has a relatively high thermal conductivity, which thus could lead to a relatively low geothermal gradient despite a high heat production.

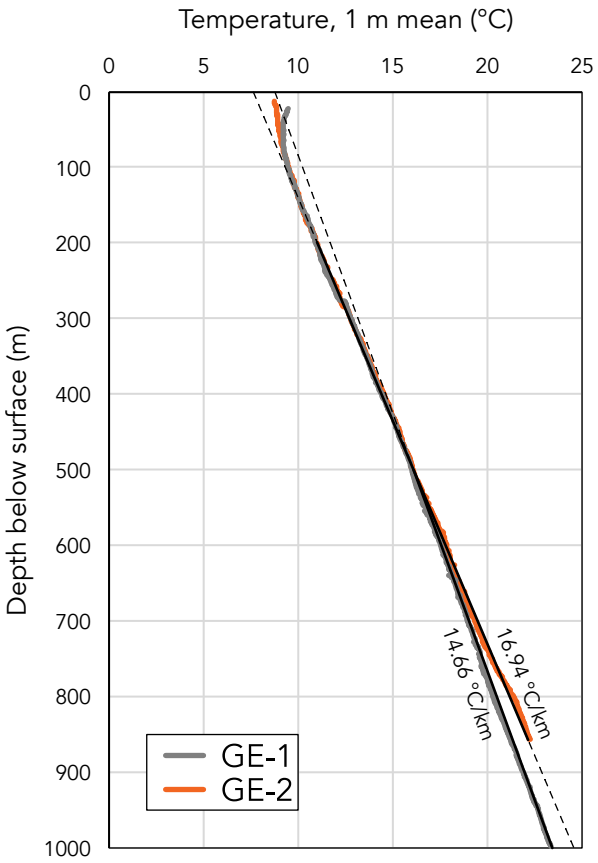


**Figure 17.** Drillhole temperature shown as a function of depth, corrected for drillhole deviation. The geothermal gradient in the upper 500 metres of GE-1 is broadly equivalent to the geothermal gradient in GE-2, but significantly lower in the deeper parts.

The measured geothermal gradient of 16.94 °C/km in GE-2 is slightly higher than expected from the average calculated thermal conductivity and radiogenic heat production of the B Group, which is approximately 15 °C/km. A simple model for the undisturbed geothermal gradient for the Gothenburg area, based on assumptions of the heat flow density and thermal properties of the crust, predicted a gradient between 17.2 and 21.3 °C/km (Angelbratt, 2020), which is close to the measured geothermal gradient in GE-2. The uncorrected apparent heat flow density in GE-2 is 53.4 mW/m², using the calculated thermal conductivity of the B Group.

Applying a palaeoclimate correction to the heat flow density (to derive the undisturbed geothermal gradient at depth) is not simple, because the climate is not stable to begin with. Different atmospheric temperature regimes, active during different periods of history and inferred from indirect temperature proxy data, have propagated down and affected the geothermal gradient to different depths and with different overlapping magnitudes. Palaeoclimate corrections to heat flow density in southern Scandinavia are in the order of 10–15 mW/m² (Majorowicz & Wybraniec, 2011). However, the magnitude of correction depends on the depth at which the heat flow density is determined, since the palaeoclimatic effect decreases exponentially with depth. The deeper the drillhole, the smaller the correction.

Comparing the uncorrected heat flow density of GE-2 with the corresponding value from the 550 m deep drillhole at Chalmers tekniska högskola (41 mW/m²), the apparent heat flow density is significantly higher at GE-2. It is therefore possible that the underlying RA granite contributes with enough radiogenic heat to significantly raise the heat flow density, which leads to a higher geothermal gradient in the overlying bedrock. On the other hand, the palaeoclimatic signal is not obvious below 200 m depth in GE-2 as the temperature trend is close to linear below 200 m (Figure 12) and even seems to decrease below 500 m in GE-1 (Figure 17).

Modelling of the heat flow density in the Gothenburg area in the Feasibility Study, based on certain assumptions about lower and upper crustal thicknesses, heat flow from the mantle, and average compositions of upper crustal rocks exposed at the surface, resulted in a value of 55.1 mW/m² (Angelbratt, 2020). Thus, the measured apparent heat flow density also could be close to the true value, since it is not far from the expected value. The

simple average corrected heat flow density in Nordic bedrock is 63 ± 2.7 mW/m² (based on 86 measured values), so even with a moderate correction for palaeoclimate, the heat flow density at GE-2 is close to the Nordic average.

With or without additional heat from the RA granite, we judge that the heat flow density and resultant geothermal gradient are close to average for Swedish crystalline bedrock. The RA granite body is likely too narrow to contribute with an amount of heat capable of significantly raising the heat flow density, as also concluded by Hogmalm *et al.* (2021). Therefore, the Gothenburg area does not contain bedrock that is more prospective in terms of a higher geothermal gradient and target temperatures at shallower depth.

If the geothermal gradient of about 17 °C/km, measured in GE-2, persists at greater depth, the target temperature of at least 120 °C (Angelbratt, 2020) would be reached at a depth of 6.6 km. This target depth is slightly deeper than the St1 Deep Heat EGS project at Otaniemi in Finland, which has the world's deepest geothermal wells at 6.4 and 6.1 km in bedrock that is similar to the crystalline gneisses in Gothenburg. The great depths of the wells at Otaniemi have proven to be a techno-economic challenge for both the construction and economic operation of an EGS power plant.

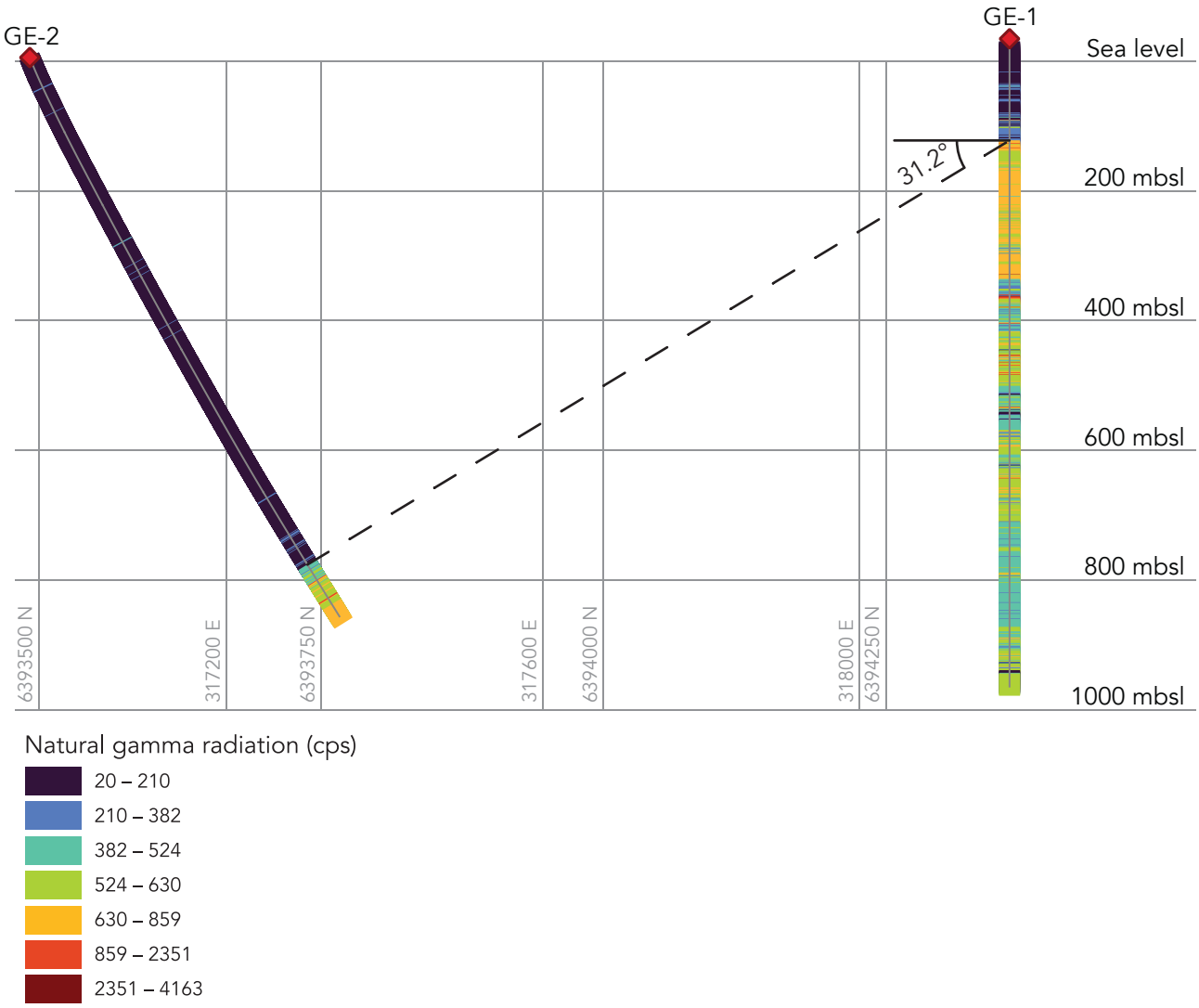


**Figure 18.** Vertical section showing GE-1 and GE-2, displaying the measured intensity of natural gamma radiation in the drillholes. Section location in Figure 8. The angle of the RA granite body is ~30° at depth.

## 7.3 Deep geology of Gothenburg

As discussed by Hogmalm *et al.* (2021), the generalised deep geological model for Gothenburg (down to 500 m) developed by Sveriges geologiska undersökning (SGU) assumes that major rock units dip approximately 50–60°

to the west. The depth of the upper contact to the RA granite in the GE-1 drill core combined with observations of the rock in the field, led to the conclusion that the large-scale structure at depth had to dip 45° or less.

The planned total depth of GE-2 was 1300 metres. At this depth, it was judged that RA granite could potentially be encountered. We aborted the drilling of GE-1 early, at a total depth of 986.65 metres. Nonetheless, from approximately 910 metres depth in the core the RA granite was intersected, as also witnessed by the downhole total natural gamma radiation intensity (Figure 18). The occurrence of RA granite in GE-2 lies much shallower than expected. A correlation between the upper contacts to the RA granite in GE-1 and GE-2 in a vertical section parallel with the direction of GE-2 and perpendicular to the regional strike of the rock units, results in a dip of approximately 30°. The observations from GE-1 and GE-2 combined, indicate that large scale geological structures observed at the surface become less steep at depth. As pointed out by Hogmalm *et al.* (2021), this adds significant uncertainty to the generalised model of the bedrock beneath Gothenburg, especially if structures such as fracture zones that are identified near the surface are to be targeted at depth.

## 8. Conclusions

The main conclusions from the investigations of GE-2, intended to answer the main aims of the project, are summarised below.

- Fractures intersected in GE-2 belong to three or four predominant fracture sets that show generally decreasing apparent frequency with depth. Of the fractures present in GE-2, the most abundant sets are smooth biotite- and chlorite-coated fractures oriented parallel to foliation planes. A set of E–W-trending fractures was intersected mainly at 300–700 m depth, corresponding to a true width of approximately 100 m with a horizontal fracture spacing of roughly 1.4 m. There is no clear indication that the intersections between the different fracture sets represent areas of increased natural permeability in the bedrock that would be prime targets for an EGS.

- The geothermal gradient from 200 m below surface to the bottom of GE-2 is 16.94 °C/km. While this is higher than the observed geothermal gradient in GE-1, it is still basically average for Swedish crystalline bedrock. Since GE-2 is underlain by the rocks with the highest heat production in the region (RA granite), it means that there does not seem to be an area with substantially increased potential for high geothermal gradients in Gothenburg compared to the average conditions in the Swedish bedrock. Since the target temperature for Göteborg Energi is 120 °C, a conventional EGS would probably need to be at least 7 km deep, which would currently make it the deepest EGS in the world. Given the techno-economic struggles of the Otaniemi EGS project, this is currently not a feasible option.

- The dip angle of large-scale structures in the bedrock underneath Gothenburg appears to become shallower with depth, as indicated by the intersection of the upper parts of the RA granite in GE-2. While general dips in the Gothenburg area at the surface are 50–60°, the angle between the top surface of the RA granite indicates a dip of approximately 30°. This means that the current near-surface knowledge of the bedrock cannot easily be extrapolated toward greater depths. If zones of increased natural permeability, such as the Göta Älv zone, were feasible targets for an EGS, a substantial amount of drilling and seismic surveys would need to be conducted in the city to construct a more accurate model of the deep geology of Gothenburg to be able to evaluate the possible location of such structures at several kilometres' depth.

## 9. Recommendations

The successful construction of an EGS depends strongly on the permeability of the rock volume between the geothermal wells. The natural permeability is rarely sufficient in crystalline bedrock. Therefore, the prospects of an EGS depend on how well the naturally occurring fractures respond to hydraulic stimulation and how well these structures can sustain the increased permeability after stimulation. This is largely an interplay between the orientation of the fractures relative to the dominant stress fields in the rock volume, which is composed of both the lithostatic pressure and tectonic forces.

If the technical constraints dictated by the geothermal gradient can be overcome, it is our recommendation that possible future investigations into the feasibility of EGS in Gothenburg should conduct hydraulic pump testing of fractures in GE-1 and GE-2 to determine the stress fields and hydraulic properties of the fractures sets.

## References


Angelbratt, A. (2020). *Feasibility study – Gothenburg affordable and fossil free Enhanced Geothermal System.*

Balling, N. (1995). Heat flow and thermal structure of the lithosphere across the Baltic Shield and northern Tornquist Zone. *Tectonophysics*, 244, 13–50.

Boehler, R. (1996). Melting Temperature of the Earth's Mantle and Core: Earth's Thermal Structure. *Annual Review of Earth and Planetary Science*, 24, 15–40.

Davies, J.H. and Davies, D.R. (2010). Earth's surface heat flux. *Solid Earth*, 1, 5–24.

Dye, S.T. (2012). Geoneutrinos and the radioactive power of the Earth. *Reviews of Geophysics*, 50, RG3007.

Foulger, G.R. (1995). The Hengill geothermal area, Iceland: Variation of temperature gradients deduced from the maximum depth of seismogenesis. *Journal of Volcanology and Geothermal Research*, 65, 119–133.

Goldschmidt, V.M. (1937). The Principles of Distribution of Chemical Elements in Minerals and Rocks. *Journal of the Chemical Society*, 1937, 655–673.

Hogmalm, J., Tillberg, M. and Angelbratt, A. (2021). *GE-1 drilling – Geological report.*

Ladefoged, J. (2021). *Structures of the deep bedrock in Gothenburg – A structural documentation of the GE1 drill core.* Bachelor of Science thesis B1138, Department of Earth Sciences, University of Gothenburg.

Larsen, N.K., Linge, H., Håkansson, L. and Fabel, D. (2011). Investigating the last deglaciation of the Scandinavian Ice Sheet in southwest Sweden with $^{10}$Be exposure dating. *Journal of Quaternary Science*, 27, 211–220.

Le Maitre, R.W., ed. (2002). *Igneous Rocks: A Classification and Glossary of Terms* (2nd edition).

Lindell, J. (2022). *A continued structural documentation of the GE-1 drill core.* Bachelor of Science thesis B1177, Department of Earth Sciences, University of Gothenburg.

Majorowicz, J. and Wybraniec, S. (2011). New terrestrial heat flow map of Europe after regional paleoclimatic correction application. *International Journal of Earth Sciences*, 100, 881–887.

McDonough, W.F. (2003). Compositional Model for the Earth's Core. *Treatise on Geochemistry* (2nd edition), 2, 547–568.

Olasolo, P., Juárez, M.C., Morales, M.P., D'Amico, S. and Liarte, I.A. (2016). Enhanced geothermal systems (EGS): A review. *Renewable and Sustainable Energy Reviews*, 56, 133–144.

Schmid, R., Fettes, D., Harte, B., Davis, E., Desmons, J., Meyer-Marsilius, H.-J. and Siivola, J. (2009). A systematic nomenclature for metamorphic rocks: 1. How to name a metamorphic rock. Recommendations by the IUGS Subcommission on the Systematics of Metamorphic Rocks.

Stanley, C.R. and Hooper, J.J. (2003). POND: an Excel spreadsheet to obtain structural attitudes of planes from oriented drillcore. *Computers & Geosciences*, 29, 531–537.

Sundberg, J., Back, P.-E., Ländell, M. and Sundberg, A. (2009). Modelling of temperature in deep boreholes and evaluation of geothermal heat flow at Forsmark and Laxemar. *SKB TR-09-14*.

Wallroth, T., Eliasson, T. and Sundquist, U. (1999). Hot dry rock research experiments at Fjällbacka, Sweden. *Geothermics*, 28, 617–625.